Title

Tunable Van Hove Singularity without Structural Instability in Kagome Metal CsTi3Bi5

Journal

Physical Review Letters, 131(2)

ISSN

0031-9007

Authors

Liu, Bo

Kuang, Min-Quan

Luo, Yang

et al.

Publication Date

2023-07-14

DOI

10.1103/physrevlett.131.026701

Tunable van Hove singularity without structural instability in Kagome metal $CsTi_3Bi_5$

Bo Liu[1,#], Minquan Kuang[2,#], Yang Luo[1,#], Yongkai Li[3,4,#], Linwei Huai[1], Shuting Peng[1], Zhiyuan Wei[1], Jianchang Shen[1], Bingqian Wang[1], Yu Miao[1], Xiupeng Sun[1], Zhipeng Ou[1], Yugui Yao[3,4], Zhiwei Wang[3,4,5,*] and Junfeng He[1,*]

[1]*Department of Physics and CAS Key Laboratory of Strongly-coupled Quantum Matter Physics, University of Science and Technology of China, Hefei, Anhui 230026, China*

[2]*Chongqing Key Laboratory of Micro & Nano Structure Optoelectronics, and School of Physical Science and Technology, Southwest University, Chongqing 400715, China*

[3]*Centre for Quantum Physics, Key Laboratory of Advanced Optoelectronic Quantum Architecture and Measurement (MOE), School of Physics, Beijing Institute of Technology, Beijing 100081, China*

[4]*Beijing Key Lab of Nanophotonics and Ultrafine Optoelectronic Systems, Beijing Institute of Technology, Beijing 100081, China*

[5]*Material Science Center, Yangtze Delta Region Academy of Beijing Institute of Technology, Jiaxing, 314011, China*

[#]These authors contributed equally to this work.

*To whom correspondence should be addressed:

J.H. (jfhe@ustc.edu.cn), Z.W.(zhiweiwang@bit.edu.cn)

In Kagome metal CsV_3Sb_5, multiple intertwined orders are accompanied by both electronic and structural instabilities. These exotic orders have attracted much recent attention, but their origins remain elusive. The newly discovered $CsTi_3Bi_5$ is a Ti-based Kagome metal to parallel CsV_3Sb_5. Here, we report angle-resolved photoemission experiments and first-principles calculations on pristine and Cs-doped $CsTi_3Bi_5$ samples. Our results reveal that the van Hove singularity (vHS) in $CsTi_3Bi_5$ can be tuned in a large energy range without structural instability, different from that in CsV_3Sb_5. As such, $CsTi_3Bi_5$ provides a complementary platform to disentangle and investigate the electronic instability with a tunable vHS in Kagome metals.

Kagome metals AV_3Sb_5 (A=K, Rb, Cs) have attracted much interest due to the coexistence of multiple exotic orders and states, ranging from superconductivity [1-3], charge density wave (CDW) [4-12], pair density wave [12], stripe order [4], nematic order [13,14], topologically nontrivial states [1,15] and time-reversal symmetry breaking states [11,16-18]. Despite the richness of these phenomena, their underlying mechanisms are still under debate. In principle, either electronic or structural instabilities of a material can drive the system into an ordered state with a lower energy. In AV_3Sb_5 (A=K, Rb, Cs), electronic instabilities are naturally provided by vHSs in the electron dispersion [19-22], and the structural instabilities are evidenced by the imaginary frequency in the phonon dispersion [23]. As a result, the explanations of the experimentally identified orders are often controversial. For example, the CDW order in AV_3Sb_5 (A=K, Rb, Cs) has been attributed to either electronic nesting between van Hove singularities [22-25] or electron-phonon coupling [26-30]; the rotational symmetry breaking has been associated with either electronic nematicity [13] or lattice modulation [14,31]. The coexisted instabilities in both electron and lattice degrees of freedom make it very challenging to identify the primary driving mechanism for the various orders in AV_3Sb_5 (A=K, Rb, Cs). In this regard, the importance of comparative studies in a parallel material system is clear. Theoretical calculations have predicted dozens of materials, which are similar to CsV_3Sb_5 [32,33]. However, ATi_3Bi_5 (A=Cs, Rb) is the only material family that has been successfully synthesized recently [34,35].

In this paper, we investigate pristine and Cs surface doped $CsTi_3Bi_5$ samples by angle-resolved photoemission spectroscopy (ARPES) and first-principles calculations. The band structure of $CsTi_3Bi_5$ is clearly revealed, which shows a clear resemblance to the calculated results. The vHS is well above Fermi level (E_F) in the pristine $CsTi_3Bi_5$. Surprisingly, the position of the vHS can be easily tuned in a large energy range by Cs surface doping. This property is distinct from that in CsV_3Sb_5, where the Cs surface doping primarily changes the Sb orbitals but has little effect on the vHS formed by V orbitals. First-principles calculations further reveal the absence of structural instability in both pristine and electron doped $CsTi_3Bi_5$. As such, our results establish $CsTi_3Bi_5$ as a complementary material platform to CsV_3Sb_5, in which the electronic instability can be systematically examined without the interference from lattice degree of freedom.

Single crystals of $CsTi_3Bi_5$ were grown by a self-flux method with binary Cs-Bi as flux. The raw materials were loaded in an alumina crucible and sealed in an evacuated quartz tube. The tube was

heated slowly to 1000 °C and held for 12 h. It was then cooled down to 850°C at a rate of 10 °C /h and to 500°C at a rate of 3°C /h, at which the flux was removed by a centrifuge. The ARPES measurements were carried out at our lab-based ARPES system using 21.2eV photons with a total energy resolution of ~5meV and a base pressure of better than 5×10^{-11} torr. The Fermi level was determined by measuring a polycrystalline Au piece in electrical contact with the samples. First-principles calculations were performed by using the VASP software package. The details of the calculations and the related parameters are described in the supplemental material.

The crystal structure of $CsTi_3Bi_5$ is similar to that of CsV_3Sb_5 (Fig. 1a). The Ti sublattice forms a Kagome net, which is interwoven with a hexagonal net of Bi atoms in the same plane. The measured band structure of $CsTi_3Bi_5$ is shown in Fig. 1b, which bears a clear resemblance to that of the first-principles calculations (Fig. 1d). Due to the layered nature of the material, a projected in-plane Brillouin zone (BZ) is used for the description. The electronic structure near the $\bar{\Gamma}$ point is dominated by an electron-like band (labelled as α band, hereafter), giving rise to a circular Fermi surface sheet (Fig. 1c). Multiple hole-like bands are observed around the $\bar{M}$ point (labelled as β, γ and δ band, respectively). They are associated with the hexagonal, flower-like and diamond-like Fermi surface sheet, respectively (Fig. 1c). A Dirac-like crossing can be seen at $\bar{K}$, and a triangular Fermi surface sheet is observed around the $\bar{K}$ point (Fig. 1c). The characteristic vHS of the Kagome lattice is shown at $\bar{M}$ point in the calculation (Fig. 1d). Nevertheless, it locates at ~150 meV above E_F, which cannot be probed by the photoemission measurements (Fig. 1d).

After revealing the overall electronic structure of the $CsTi_3Bi_5$, we now investigate the doping evolution via *in situ* surface deposition of Cs atoms. As shown in Fig. 2a, the electron-like band (α band) around $\bar{\Gamma}$ shows a moderate change as a function of Cs doping (Fig. 2a). The distance between the two Fermi momenta (k_{F1} and k_{F2}) increases slightly with doping (Fig. 2b). On the contrary, the energy bands around $\bar{M}$ exhibit more significant changes as a function of Cs doping (Fig. 2d). In particular, the γ and δ bands present a clear downward shift, echoing the expected electron doping with Cs surface deposition. We note that the top of these hole-like bands starts to appear with sufficient Cs doping [Fig. 2d(v)], indicating that the vHS is in the vicinity of E_F. This is also evidenced by the enhanced electron density of states at E_F in this momentum region (Fig. 2e, f). The integrated energy distribution curve (EDC) around the $\bar{M}$ point shows a negligible peak in the pristine $CsTi_3Bi_5$,

as the vHS is well above E_F (Fig. 2e). However, the peak intensity increases significantly with Cs doping, demonstrating the boost of low energy electron density of states as the vHS approaches E_F (Fig. 2f). In order to quantitatively unveil the vHS, the Cs surface doping is reproduced at an elevated temperature (T=200K), where the thermal population of electrons enables a complete examination of the fine features around E_F. As shown in Fig. 3a-d, the vHS is indeed shifted downward with doping. On the sufficiently doped sample, the flat dispersion of the vHS can be clearly identified in the vicinity of E_F (Fig. 3b, d). These results are quantitatively extracted from the data and summarized in Fig. 3f. Orbital-resolved calculations have also been carried out, which illustrate that the electron-like α band around $\bar{\Gamma}$ is dominated by Bi P_z orbital, whereas the vHS is primarily associated with Ti $d_{x^2-y^2}$ orbital (Fig. 3e). These observations have collectively depicted an integrated picture of orbital selective movements of the energy bands with Cs doping -- the vHS with Ti *d* orbitals can be tuned in a large energy range, whereas the electron-like α band with Bi *P* orbitals remains less sensitive to the doping process. This is distinct from the evolution in CsV_3Sb_5, where the vHS with V *d* orbitals shows little change with Cs surface doping, but the electron-like band with Sb *P* orbitals shifts ~240 meV in energy [36].

Next, we examine the lattice degree of freedom in the $CsTi_3Bi_5$ crystal. We have followed the idea in CsV_3Sb_5 [23], and calculated the change of total energy in $CsTi_3Bi_5$, assuming that the lattice is breathing in and out towards the potential Star of David (SD) and inverse Star of David (ISD) structures (Fig. 4a). In CsV_3Sb_5, either SD or ISD structure shows a lower total energy than that of the Kagome structure (Fig. 4b), leading to structural instabilities of the material [23]. On the contrary, the Kagome structure in $CsTi_3Bi_5$ exhibits the lowest total energy, demonstrating the absence of structural instability (Fig. 4c). This result remains solid when electron doping is considered in the $CsTi_3Bi_5$ system (Fig. 4d). Phonon spectra are also calculated for both pristine and electron doped $CsTi_3Bi_5$ (Fig. 4e). The absence of imaginary frequency echoes a stable Kagome structure in $CsTi_3Bi_5$.

Finally, we discuss the implications of our observations. The tunable vHS and the absence of structural instabilities make $CsTi_3Bi_5$ a complementary material platform to compare with CsV_3Sb_5. Without the interference from lattice, one can systematically examine the electronic instabilities associated with the vHS. For example, the CDW order is absent in the pristine $CsTi_3Bi_5$ [34,35], and no CDW gap is observed in our ARPES measurements (see supplemental material). When the vHS is tuned to the vicinity of E_F, the photoemission spectra remain gapless at low temperature (see

supplemental material). There results indicate that the electronic nesting between vHSs at $\bar{M}$ points is insufficient to drive a CDW order in the Kagome metal. The structural instabilities in CsV_3Sb_5 play an essential role in this context. On the other hand, nematic order might be driven by pure electronic interactions, as it has been reported in both CsV_3Sb_5 and $CsTi_3Bi_5$ [13,14,37,38]. It would be interesting to further explore how the tunable vHS in $CsTi_3Bi_5$ would interact with the nematic order and other potential electronic orders in the system.

In summary, we have revealed the electronic structure of pristine and Cs surface doped $CsTi_3Bi_5$ samples. The Cs deposition induces an overall electron doping to the material, but the energy bands exhibit an orbital dependent movement with doping. Among them, the vHS can be tuned in a large energy range. First-principles calculations demonstrate that the Kagome structure remains stable in both pristine and electron doped $CsTi_3Bi_5$. These results establish a unique path to disentangle the electronic instability from that of the lattice, and to examine its relationship with the various exotic phenomena in Kagome metals.

[1] B. R. Ortiz, S. M. L. Teicher, Y. Hu, J. Zuo, P. M. Sarte, E. C. Schueller, A. M. M. Abeykoon, M. J. Krogstad, S. Rosenkranz, R. Osborn, R. Seshadri, L. Balents, J. He, and S. D. Wilson, Phys. Rev. Lett. **125**, 247002 (2020).

[2] B. R. Ortiz, P. M. Sarte, E. M. Kenney, M. J. Graf, S. M. L. Teicher, R. Seshadri, and S. D. Wilson, Phys. Rev. Mater. **5**, 034801 (2021).

[3] Q. Yin, Z. Tu, C. Gong, Y. Fu, S. Yan, and H. Lei, Chin. Phys. Lett. **38**, 037403 (2021).

[4] H. Zhao, H. Li, B. R. Ortiz, S. M. L. Teicher, T. Park, M. Ye, Z. Wang, L. Balents, S. D. Wilson, and I. Zeljkovic, Nature (London) **599**, 216-221 (2021).

[5] Z. Liang, X. Hou, F. Zhang, W. Ma, P. Wu, Z. Zhang, F. Yu, J.-J. Ying, K. Jiang, L. Shan, Z. Wang, and X.-H. Chen, Phys. Rev. X **11**, 031026 (2021).

[6] H. Li, T. T. Zhang, T. Yilmaz, Y. Y. Pai, C. E. Marvinney, A. Said, Q. W. Yin, C. S. Gong, Z. J. Tu, E. Vescovo, C. S. Nelson, R. G. Moore, S. Murakami, H. C. Lei, H. N. Lee, B. J. Lawrie, and H. Miao, Phys. Rev. X **11**, 031050 (2021).

[7] B. R. Ortiz, S. M. L. Teicher, L. Kautzsch, P. M. Sarte, N. Ratcliff, J. Harter, J. P. C. Ruff, R. Seshadri, and S. D. Wilson, Phys. Rev. X **11**, 041030 (2021).

[8] F. H. Yu, D. H. Ma, W. Z. Zhuo, S. Q. Liu, X. K. Wen, B. Lei, J. J. Ying, and X. H. Chen, Nat. Commun. **12**, 3645 (2021).

[9] Y. Song, T. Ying, X. Chen, X. Han, Y. Huang, X. Wu, A.P. Schnyder, J. Guo, and X. Chen, Phys. Rev. Lett. **127**, 237001 (2021).

[10] B. Q. Song, X. M. Kong, W. Xia, Q. W. Yin, C. P. Tu, C. C. Zhao, D. Z. Dai, K. Meng, Z. C. Tao, Z. J. Tu, C. S. Gong, H. C. Lei, Y. F. Guo, X. F. Yang, and S. Y. Li, arXiv:2105.09248 (2021).

[11] Y.-X. Jiang, J.-X. Yin, M. M. Denner, N. Shumiya, B. R. Ortiz, G. Xu, Z. Guguchia, J. He, M. S. Hossain, X. Liu, J. Ruff, L. Kautzsch, S. S. Zhang, G. Chang, I. Beloposki, Q. Zhang, T. A. Cochran, D. Multer, M. Litskevich, Z.-J. Cheng, X. P. Yang, Z. Wang, R. Thomale, T. Neupert, S. D. Wilson, and M. Z. Hasan, Nat. Mater. **20**, 1353-1357 (2021).

[12] H. Chen, H. Yang, B. Hu, Z. Zhao, J. Yuan, Y. Xing, G. Qian, Z. Huang, G. Li, Y. He, S. Ma, S. Ni, H. Zhang, Q. Yin, C. Gong, Z. Tu, H. Lei, H. Tan, S. Zhou, C. Shen, X. Dong, B. Yan, Z. Wang, and H.-J. Gao, Nature (London) **599**, 222-228 (2021).

[13] L. Nie, K. Sun, W. Ma, D. Song, L. Zheng, Z. Liang, P. Wu, F. Yu, J. Li, M. Shan, D. Zhao, S. Li, B. Kang, Z. Wu, Y. Zhou, K. Liu, Z. Xiang, J. Ying, Z. Wang, T. Wu, and X. Chen, Nature (London) **604**, 59-64 (2022).

[14] Y. Xiang, Q. Li, Y. Li, W. Xie, H. Yang, Z. Wang, Y.Yao, H.-H. Wen, Nat. Commun. **12**, 6727 (2021).

[15] Y. Hu, S. M. L. Teicher, B. R. Ortiz, Y. Luo, S. Peng, L. Huai, J. Ma, N. C. Plumb, S. D. Wilson, J. He, and M. Shi, Sci. Bull. **67**, 495 (2022).

[16] C. M. III, D. Das, J.-X. Yin, H. Liu, R. Gupta, Y.-X. Jiang, M. Medarde, X. Wu, H. C. Lei, J. Chang, P. Dai, Q. Si, H. Miao, R. Thomale, T. Neupert, Y. Shi, R. Khasanov, M. Z. Hasan, H. Luetkens, and Z. Guguchia, Nature (London) **602**, 245-250 (2022).

[17] L. Yu, C. Wang, Y. Zhang, M. Sander, S. Ni, Z. Lu, S. Ma, Z. Wang, Z. Zhao, H. Chen, K. Jiang, Y. Zhang, H. Yang, F. Zhou, X. Dong, S. L. Johnson, M. J. Graf, J. Hu, H. J. Gao, Z. Zhao, arXiv:2107.10741.

[18] R. Khasanov, D. Das, R. Gupta, C. Mielle, M. Elender, Q. Yin, Z. Tu, C. Gong, H. Lei, E. T. Ritz, R. M. Fernandes, T. Birol, Z. Guguchia, and H. Luetkens, Phys. Rev. Res. **4**, 023224 (2022).

[19] M. Kang, S. Fang, J.-K. Kim, B. R. Ortiz, S. H. Ryu, J. Kim, J. Yoo, G. Sangiovanni, D. D. Sante, B.-G. Park, C. Jozwiak, A. Bostwick, E. Rotenberg, E. Kaxiras, S. D. Wilson, and J.-H. Park, R. Comin, Nat. Phys. **18**, 301-308 (2022).

[20] Y. Hu, X. Wu, B. R. Ortiz, S. Ju, X. Han, J. Ma, N. C. Plumb, M. Radovic, R. Thomale, S. D. Wilson, A. P. Schnyder, and M. Shi, Nat. Commun. **13**, 2220 (2022).

[21] Z. Liu, N. Zhao, Q. Yin, C. Gong, Z. Tu, M. Li, W. Song, Z. Liu, D. Shen, Y. Huang, K. Liu, H. Lei, S. Wang, Phys. Rev. X **11**, 041010 (2021).

[22] S. Cho, H. Ma, W. Xia, Y. Yang, Z. Liu, Z. Huang, Z. Jiang, X. Lu, J. Liu, Z. Liu, J. Li, J. Wang, Y. Liu, J. Jia, Y. Guo, J. Liu, and D. Shen, Phys. Rev. Lett. **127**, 236401 (2021).

[23] H. Tan, Y. Liu, Z. Wang, and B. Yan, Phys. Rev. Lett. **127**, 046401 (2021).

[24] R. Lou, A. Fedorov, Q. Yin, A. Kuibarov, Z. Tu, C. Gong, E.F. Schwier, B. Buchner, H. Lei, and S. Borisenko, Phys. Rev. Lett. **128** 036402 (2022).

[25] X. Zhou, Y. Li, X. Fan, J. Hao, Y. Dai, Z. Wang, Y. Yao, and H. Wen, Phys. Rev. B **104**, L041101 (2021).

[26] H. Luo, Q. Gao, H. Liu, Y. Gu, D. Wu, C. Yi, J. Jia, S. Wu, X. Luo, Y. Xu, L. Zhao, Q. Wang, H. Mao, G. Liu, Z. Zhu, Y. Shi, K. Jiang, J. Hu, Z. Xu, and X.J. Zhou, Nat. Commun. **13**, 273 (2022).

[27] E. Uykur, B. R. Ortiz, S. D. Wilson, M. Dressel, and A. A. Tsirlin, npj Quantum Mater. **7**, 16 (2022).

[28] Y. Xie, Y. Li, P. Bourges, A. Ivanov, Z. Ye, J. Yin, M.Z. Hasan, A. Luo, Y. Yao, Z. Wang, G, Xu, and P. Dai, Phys. Rev. B **105**, L140501 (2022).

[29] Z. Ye, A. Luo, J.-X. Yin, M.Z. Hasan, and G. Xu, Phys. Rev. B **105**, 245121 (2022).

[30] M. Wenzel, B. R. Ortiz, S. D. Wilson, M. Dressel, A. A. Tsirlin, and E. Uykur, arXiv:211207501 (2021).

[31] Z. Jiang, H. Ma, W. Xia, Q. Xiao, Z. Liu, Z. Liu, Y. Yang, J. Ding, Z. Huang, J. Liu, Y. Qiao, J. Liu, Y. Peng, S. Cho, Y. Guo, J. Liu, and D. Shen, arXiv:2208.01499 (2022).

[32] Y. Jiang, Z. Yu, Y. Wang, T. Lu, S. Meng, K. Jiang, and M. Liu, Chin. Phys. Lett. **39**, 047402 (2022).

[33] X.-W. Yi, X.-Y. Ma, Z. Zhang, Z.-W. Liao, J.-Y. You, G. Su, arXiv:2202.05588 (2022).

[34] H. Yang, Z. Zhao, X.-W. Yi, J. Liu, J.-Y. You, Y. Zhang, H. Guo, X. Lin, C. Shen, H. Chen, X. Dong, G. Su, H.-J. Gao, arXiv:2209.03840 (2022).

[35] D. Werhahn, B. R. Ortiz, A. K. Hay, S. D. Wilson, R. Seshadri, S. Johrendt, Zeitschrift für Naturforsch. B online (2022). doi:10.1515/znb-2022-0125.

[36] K. Nakayama, Y. Li, T. Kato, M. Liu, Z. Wang, T. Takahashi, Y. Yao, and T. Sato, Phys. Rev. X **12**, 011001 (2022).

[37] H. Yang, Y. Ye, Z. Zhao, J. Liu, X.-W. Yi, Y. Zhang, J. Shi, J. Y. You, Z. Huang, B. Wang, J. Wang, H. Guo, X. Lin, C. Shen, W. Zhou, H. Chen, X. Dong, Z. Wang, H.J. Gao, arXiv:2211.12264 (2022).

[38] H. Li, S. Cheng, B. R. Ortiz, H. Tan, D. Werhahn, K. Zeng, D. Jorhendt, B. Yan, Z. Wang, S. D. Wilson, I. Zeljkovic, arXiv:2211.16477 (2022).

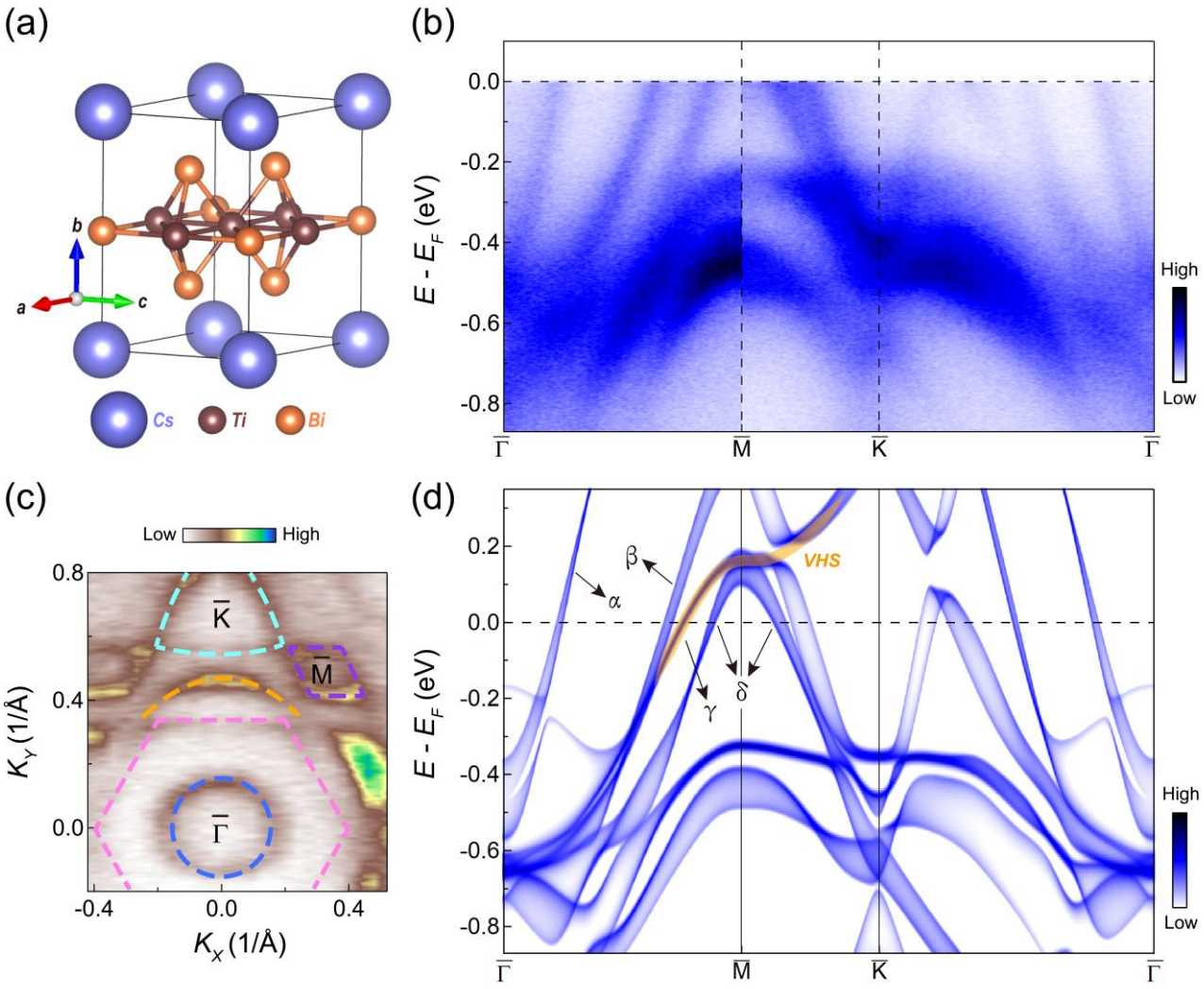

FIG. 1. Electronic structure of $CsTi_3Bi_5$. (a) Crystal structure of $CsTi_3Bi_5$. (b-c) Photoelectron intensity plot along $\bar{\Gamma}$-$\bar{M}$-$\bar{K}$-$\bar{\Gamma}$ (b) and Fermi surface (c) of $CsTi_3Bi_5$ measured with 21.2 eV photons at 7K. The dashed lines in (c) are a guide to the eye. (d) The bulk band structure of $CsTi_3Bi_5$ obtained from first-principles calculations with spin-orbital coupling included. The electron-like band around $\bar{\Gamma}$ and the hole-like bands near $\bar{M}$ are labelled as α, β, γ and δ band, respectively. The orange shade is an eye-guide for the vHS.

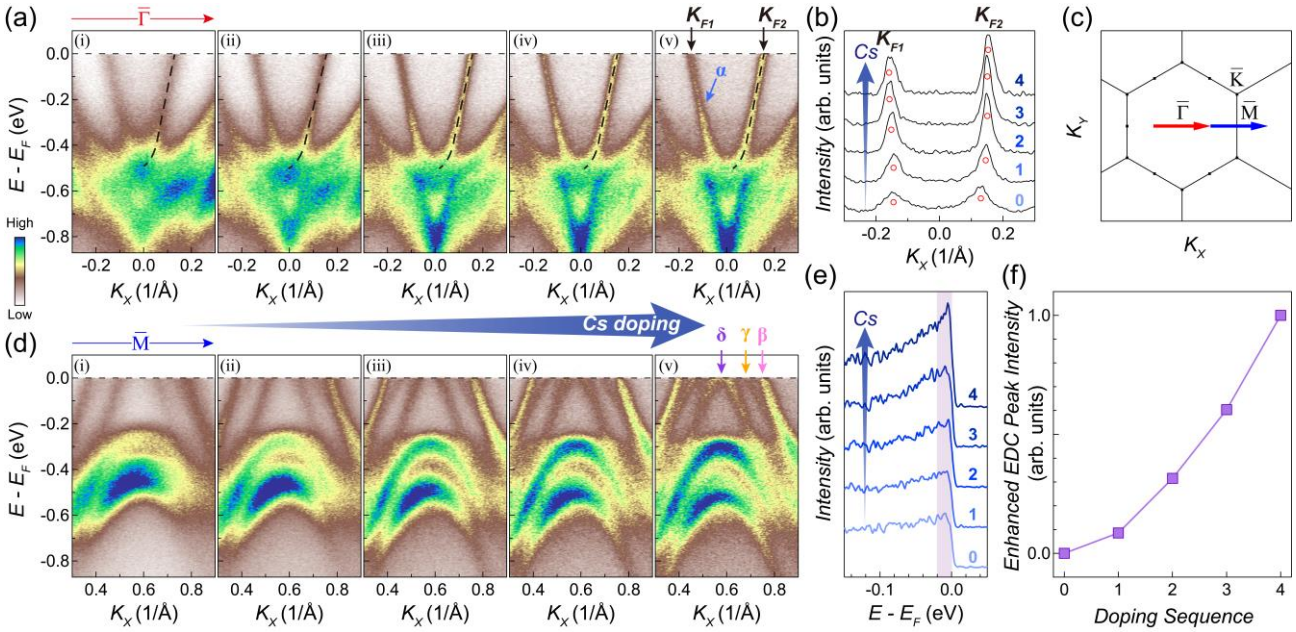

FIG. 2. Evolution of the electronic structure with Cs surface doping at 7K. (a) Photoelectron intensity plot of the band structure around $\bar{\Gamma}$ as a function of continuous Cs doping on the same sample. The results at doping sequences 0-4 are shown in (i-v), respectively. Doping sequence 0 indicates the pristine $CsTi_3Bi_5$ sample. The dashed lines are a guide to the eye. (b) Momentum distribution curves (MDCs) at E_F extracted from (a). (c) The projected in-plane BZ and the momentum locations of the cuts. (d) Same as (a), but for the band structure around $\bar{M}$. (e) Integrated EDC around the $\bar{M}$ point in (d). The numbers 0-4 denote the doping sequences. (f) Enhanced EDC peak intensity around $\bar{M}$ as a function of the doping sequence. The absolute EDC peak intensity at the doping sequence x (x=0-4) is calculated by integrating the area between -20meV and E_F of the corresponding EDC, and labelled as I_x. The enhanced EDC peak intensity is defined as $(I_x-I_0)/(I_4-I_0)$.

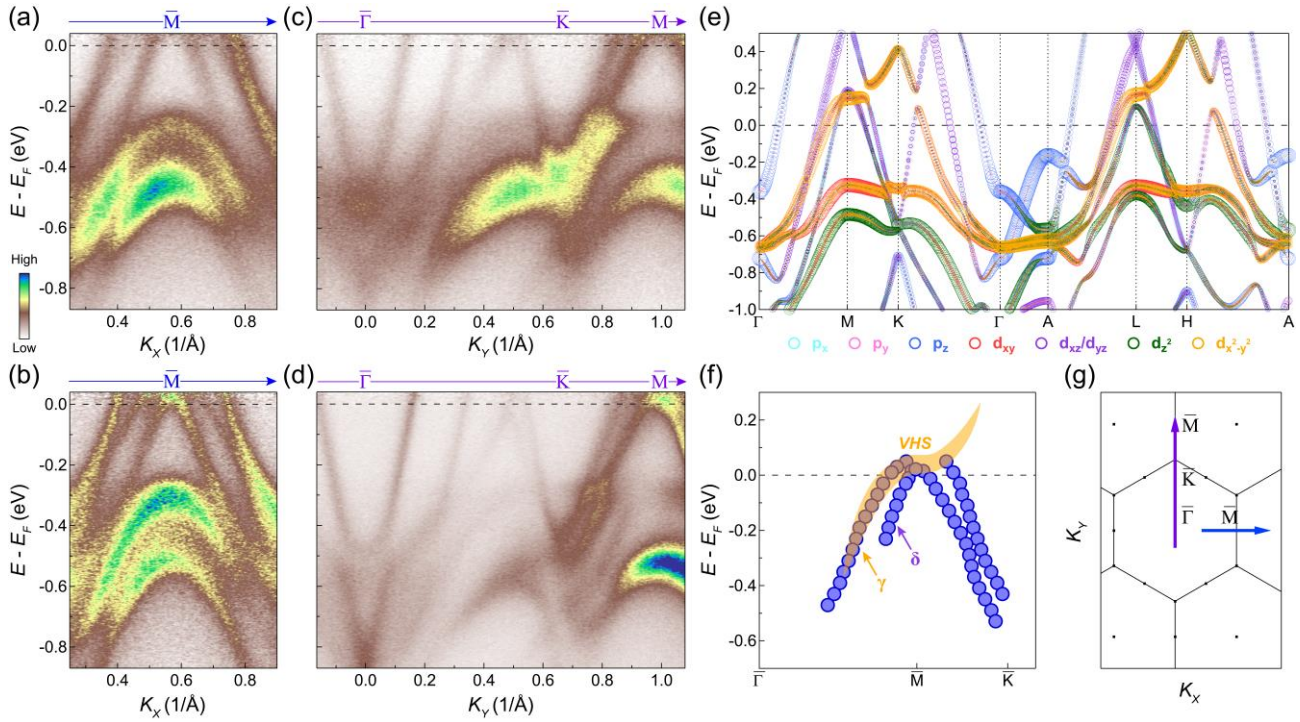

FIG. 3. Doping evolution of the vHS. (a-b) Photoelectron intensity plot of the band structure around $\bar{M}$ (along the $\bar{\Gamma}$-$\bar{M}$-$\bar{\Gamma}$ direction) before (a) and after (b) the Cs surface doping, measured at 200K. (c-d) Same as (a-b), but measured along the $\bar{\Gamma}$-$\bar{K}$-$\bar{M}$ direction. (e) Orbital-resolved band structure obtained by first-principles calculations. (f) Quantified dispersion of the γ and δ bands near $\bar{M}$ after sufficient Cs doping, extracted from (b) and (d). The orange shade is an eye-guide for the vHS. (g) Momentum locations of the cuts in the BZ.

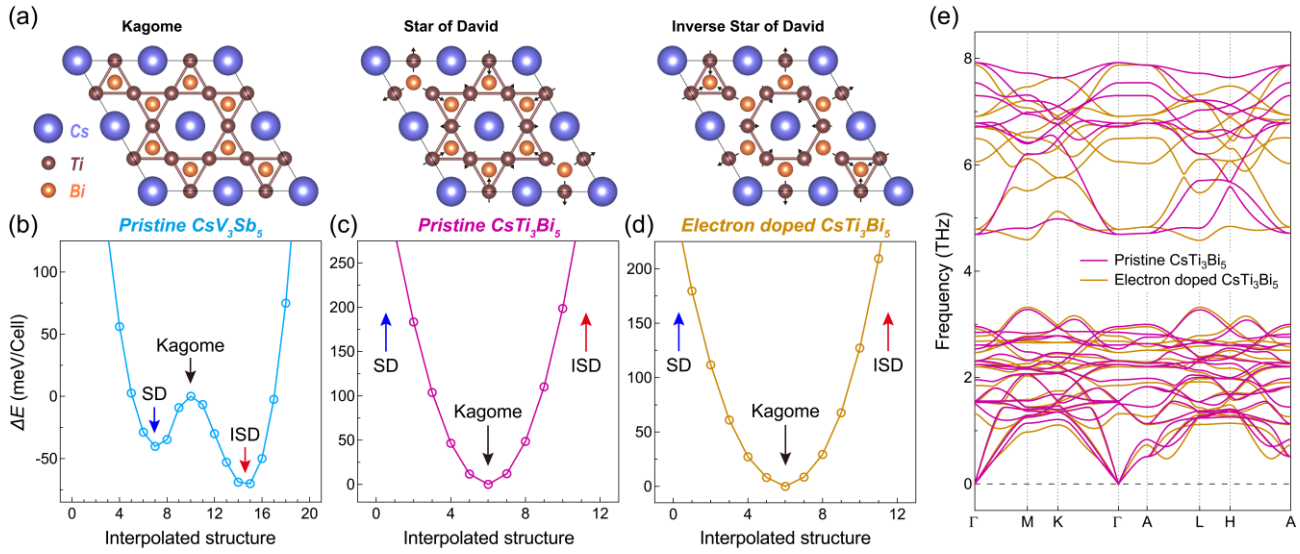

FIG. 4. Calculated total energy profiles and phonon spectra. (a) The 2×2 supercells for Kagome structure, Star of David structure and Inverse Star of David structure. The black arrows indicate the lattice distortion due to the breathing mode. (b-d) Total energy as a function of the interpolated structure in pristine CsV_3Sb_5 (b), pristine $CsTi_3Bi_5$ (c), and electron doped $CsTi_3Bi_5$ (d). (e) Calculated phonon spectra along the high-symmetry directions in pristine $CsTi_3Bi_5$ (magenta line) and electron doped $CsTi_3Bi_5$ (orange line).